Journal of Magnetism and Magnetic Materials 473 (2019) 495–500

Contents lists available at ScienceDirect

Journal of Magnetism and Magnetic Materials

journal homepage: www.elsevier.com/locate/jmmm

Research articles

Actuation and visualization of a magnetically coated swimmer with magnetic particle imaging

Anna C. Bakenecker[a,*], Anselm von Gladiss[a], Thomas Friedrich[a], Ulrich Heinen[b,c], Heinrich Lehr[c], Kerstin Lüdtke-Buzug[a], Thorsten M. Buzug[a]

[a] Institute of Medical Engineering, University of Lübeck, Ratzeburger Allee 160, 23562 Lübeck, Germany
[b] Dept. of Electrical Engineering & Information Technology, Pforzheim University of Applied Sciences, Tiefenbronner Strasse 65, 75175 Pforzheim, Germany
[c] Bruker BioSpin MRI GmbH, Rudolf-Plank-Str. 23, 76275 Ettlingen, Germany

ARTICLE INFO

Keywords:
Magnetic particle imaging
MPI
Superparamagnetic nanoparticles
Magnetic actuation
Millirobotics

ABSTRACT

The untethered actuation of milli- and microdevices is of great interest for a variety of medical applications. A millimeter sized swimmer is shown, which is 3D-printed and coated with magnetic nanoparticles. The coating has to fulfill two requirements: First, it must have a high magnetic moment in order to show a strong reaction to a magnetic field for good actuation performance. Second, it has to be suitable for magnetic particle imaging (MPI). MPI is an emerging medical imaging technique, based on the nonlinear response of superparamagnetic nanoparticles to oscillating magnetic fields. It is aimed at dual use of an MPI scanner: for both actuation and visualization. When applying rotating homogeneous magnetic fields, the swimmer performs an axial movement due to its shape and the viscosity of the surrounding medium. These fields can be generated with an MPI scanner. The swimmer dynamics have been observed and a maximum swimming velocity of 6 mm/s at a rotation frequency of the magnetic field of 10 Hz was found. The experiments are performed with a commercially available preclinical MPI scanner. It is shown, that the swimmer is suitable to be imaged with MPI. Furthermore, sequentially acquired images of a moving swimmer are shown. For this, the MPI scanner was alternately driven in imaging and actuation mode.

1. Introduction

Magnetic actuation of medical devices, such as catheters, small cameras or drug filled capsules, enables to improve the precision of minimally invasive surgery. Catheters can be steered towards the region of interest. A commercially available manipulation system consisting of permanent magnets is already available (Stereotaxis Niobe). Drugs can be delivered directly to cancerous tissue or inflammatory regions with endoscopic capsules, which allows lower dosages. Furthermore, healthy tissue is less affected [1,2]. The gastrointestinal tract can be investigated using untethered, swallowable video capsules, that are steerable with external magnetic fields [3,4]. Another application is to take a biopsy by using a magnetically steerable capsule equipped with a biopsy needle. This way, biopsies can be taken out of tissue regions difficult to access without surgery [5–7]. Smaller magnetic swimmers of micrometer size can be also steered through the vascular system, urinary system or organs difficult to access, such as the ear or the eye [8]. Several approaches have shown the possibility to produce micrometer sized helical swimmers containing magnetic nanoparticles, which can be directed to the region of interest by homogeneous rotating magnetic fields [9–11]. To visualize the actuation, different well established imaging techniques are used [8]. Usually, the aforementioned magnetic milli- and micrometer sized robots are visualized by optical imaging techniques, such as video, light or fluorescence microscopy [9,12,13]. These imaging techniques are suitable for *in vitro* experiments, since they are non tomographic. Further, tomographic imaging techniques have been used such as ultrasound, X-ray, computed tomography, magnetic resonance imaging or hall-effect sensor arrays [4]. Magnetic particle imaging (MPI) is an emerging tomographic imaging technique enabling 3D real-time imaging of magnetic material [14,15]. Usually, superparamagnetic iron oxide nanoparticles are used as tracer material. The advantage of visualizing magnetic actuation with MPI is that the magnetic fields of existing MPI scanners can be used for actuation, and therefore, no external imaging technique has to be integrated into the actuation setup. Further, MPI enables radiation free tomographic imaging, it is highly sensitive and has the potential of submillimeter resolution [14,15]. It has been shown that magnetic particles can be moved using the magnetic gradient field of an MPI scanner [16–20].

* Corresponding author.
E-mail addresses: bakenecker@imt.uni-luebeck.de (A.C. Bakenecker), buzug@imt.uni-luebeck.de (T.M. Buzug).

https://doi.org/10.1016/j.jmmm.2018.10.056
Received 24 June 2018; Received in revised form 11 October 2018; Accepted 11 October 2018
Available online 12 October 2018
0304-8853/

Macroscopic devices such as catheters and screws can be navigated inside an MPI scanner [21–24]. These investigations show the potential of combining the actuation of magnetic swimmers with MPI.

2. Theory

The magnetic force on a magnetizable object in a magnetic gradient field $\nabla\vec{B}_G$ can be expressed as

$$\vec{F} = \vec{m}\cdot\nabla\vec{B}_G, \tag{1}$$

with $\vec{m}$ being the magnetic moment and $\vec{M} = \frac{\vec{m}}{V}$ the magnetization of the object of volume V, when assuming a homogeneous magnetization of the object. Since the magnetic moment aligns with the magnetic field, this leads to a movement of the object towards a higher field strength. For magnetic actuation, objects of large magnetic moments are required. Setups featuring large field gradients are necessary in order to actuate even very small objects.

Furthermore, it is possible to induce a torque on a magnetizable object, which means that the object's magnetic moment aligns with a homogeneous magnetic field

$$\vec{T} = \vec{m}(t) \times \vec{B}_{\mathrm{rot}}(t). \tag{2}$$

If the direction of the homogeneous field rotates, i.e. having the form

$$\vec{B}_{\mathrm{rot}}(t) = \begin{pmatrix} 0 \\ \pm B_F^y \cos(\omega_F t) \\ - B_F^z \sin(\omega_F t) \end{pmatrix}, \tag{3}$$

the object rotates with the same frequency [25,8,26,27]. The magnetic field in Eq. (3) rotates either left or right handed in the yz-plane, leading to a rotation of the object around the x-axis. The field amplitudes are called B_F, as they are generated by the focus fields of the MPI system (see Section 2.2).

2.1. Swimmer dynamics

Full rotation of the swimmer can be only expected within a certain frequency range of the applied magnetic field, which depends on the object's size, shape and magnetic moment. For small frequencies the swimmer prefers to rotate around the short axis, leading to a "tumbling" motion and no axial movement. When increasing the frequency, the swimmer changes to a "wobbling" motion, which is a precession around the long axis. Finally, it fulfills a "corkscrew" motion at higher frequencies, leading to the highest axial velocities of the swimmer [28]. This behavior can be explained as a competition between the magnetic torque (see Eq. (2)) and the viscous friction. The faster the object rotates, the more friction it experiences. A rotation around the long axis of the swimmer reduces the friction and therefore, it is energetic preferable. At very high frequencies the viscous friction is larger than the magnetic torque and therefore, no rotation can be observed. This frequency is called "step out frequency" [29].

2.2. Magnetic particle imaging

MPI is based on the nonlinear response of magnetic nanoparticles to an applied varying magnetic field [14,30,31]. Sinusoidal drive fields produce harmonic components, which get visible in the frequency domain of the measured time signal. To spatially encode the particle signal, a gradient field, featuring a field free region, is applied. Only particles within and nearby the field free region contribute to the signal, which enables the spatial localization of the received particle signal. The field of view is defined by the drive field strength and the gradient. It is possible to quantitatively image the distribution of a tracer material, for which usually superparamagnetic iron oxide nanoparticles are used. MPI is highly sensitive to very small amounts of iron [32] and features 3D real-time imaging with submillimeter resolution [15]. The system matrix approach has been chosen to reconstruct the images [14]. It utilizes the Kaczmarz algorithm to reconstruct the spatial distribution of the particles. The system matrix stores the particle response of a certain type of particles and imaging sequence for each voxel in the field of view. The aim is to solve the equation $Sc = u$ for the particle distribution c, with S being the system matrix and u the particle signal [33]. To further enlarge the field of view, homogeneous offset fields can be used, which are called focus fields [34]. These fields shift the scanned volume in space.

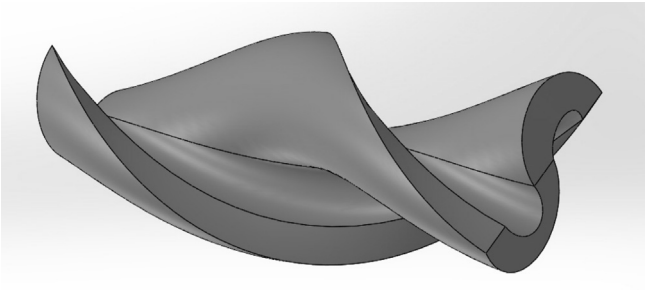

Fig. 1. CAD-Model of the swimmer having a savonius shape.

3. Methods and materials

3.1. Magnetically coated swimmer

The swimmer is 3D-printed (Projet 3510 HD+) using the printing material VisiJet®X (3D Systems), a polymer resin. The swimmer has a savonius shape (see Fig. 1) with a diameter of 1.8 mm and a length of 4.5 mm. The swimmer is painted with multiple layers of a mixture of acrylic paint and Perimag nanoparticles (water-soluble, 130 nm, dextran coated, Micromod). A 7: 5 mass ratio of acrylic paint to nanoparticle solution was experimentally determined to provide sufficient MPI signal without diluting the paint too much. To enhance steerability through an increased magnetic moment, a final layer of acrylic lacquer with a 25 mass-% admixture of iron (II,III) oxide powder (50 − 100 nm, Sigma Aldrich) was added. This particle concentration is still below the onset of agglomeration.

3.2. Magnetic particle imaging scanner

The experiments are performed with a commercially available preclinical MPI scanner (Bruker Biospin MPI 25/20 FF). It features a gradient field forming a field free point (FFP) with a gradient strength of up to 2.5 T/m in the z-direction (vertical) and 1.25 T/m in the x- and y-direction. The drive field has a maximum strength of 12 mT in the x-, y- and z-direction. When applying these settings a field of view of $19.2 \times 19.2 \times 9.6\ \mathrm{mm}^3$ is achieved. The different drive field frequencies are about 25 kHz. To enlarge the field of view, focus fields of up to 18 mT in the x- and y-direction and 42 mT in the z-direction can be applied.

3.3. Actuation

By applying sinusoidal currents with a 90° phase shift to two focus field coils, a rotating magnetic field vector with a rotation frequency of up to 50 Hz can be generated. These rotating focus fields can be used to manipulate magnetic material inside the MPI scanner (see Eqs. (2) and (3)). In the actuation mode different rotation frequencies of up to 20 Hz and focus field strengths of up to 18 mT were used. The swimmer is put into two different water filled phantoms. One is a glass cylinder of 5 cm length, the other is a Y-shaped 3D-printed vessel phantom The branches have a length of 1.5 cm each and a diameter of 4 mm (see Fig. 2). To steer the swimmer in different directions the orientation of the rotating

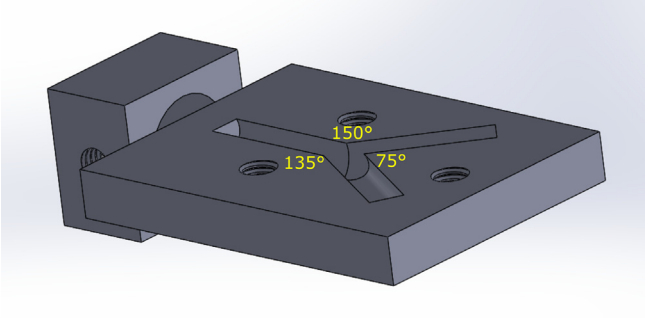

Fig. 2. CAD-Model of the vessel phantom, the angles between the branches are indicated. The length of each branch is 1.5 cm and the diameter is 4 mm.

magnetic field can be changed to arbitrary rotating planes. The actuation is verified by a video camera which is placed above the phantoms inside the scanner bore. The camera needs to be removed during the MPI sequence (see Section 3.4).

3.4. Visualization

To proof the suitability of the swimmer for MPI, a 3D frequency spectrum was acquired with the preclinical MPI scanner. The x-, y- and z- drive field strength was set to 12 mT. To compare the swimmer signal with a pure particle sample, 10 µl of undiluted Perimag was measured as well. Since the measured spectra are influenced by background disturbances of the system, a measurement of the empty bore needs to be acquired with the same scanning parameters. Then, the empty measurement can be subtracted from the measured data for coping with the stationary background of the scanner. When performing both actuation and visualization, an MPI image was taken after every 10 turns of the swimmer. In the imaging mode a drive field in the x- and y-direction of 12 mT and a gradient field of 1.5 T/m in the z-direction and 0.75 T/m in the x- and y-direction was applied, leading to a 2D field of view of $32 \times 32\ mm^2$. The image acquisition time was 3.246 s and the number of averages was 5000. The image is reconstructed with a 57×57 system matrix. The frequency range chosen for reconstruction was between 80 kHz and 1.25 MHz. Using an SNR threshold of 20, 91 frequency components were chosen for reconstruction. For the regularized Kaczmarz reconstruction algorithm, the number of iterations was set to 3 and the regularization parameter was set to 0.05. It has to be mentioned that there is a time delay of about 30 s between the imaging mode and the actuation mode. This is the time the system needs to ramp up the drive fields, which is a current software limitation.

4. Results and discussion

4.1. Actuation

The swimmer rotates at frequencies of up to 14 Hz and fulfills an axial movement when applying a frequency between 4 Hz and 14 Hz. At 10 Hz it travels with a speed of approximately 6 mm/s (see Fig. 3 and the Supplementary material [video:SwimmerGlasPhantom]). At this frequency the swimmer travels in a “corkscrew” motion, leading to maximum velocities. For frequencies larger than 14 Hz no rotation can be observed. For frequencies smaller than approximately 8 Hz, a “wobbling” motion can be observed (see Section 2.1). A video demonstrating the swimmer dynamics for different frequencies can be found in the Supplementary material [video:SwimmerDynamics]. Furthermore, the swimmer could be steered through the vessel phantom at a rotation frequency of 10 Hz (see Fig. 4 and the video in the Supplementary material [video:SwimmerVesselPhantom]). By changing the plane of rotation it is possible to steer the swimmer in arbitrary directions and therefore, through all the branches of a vessel phantom. The indicated frequency range for a “corkscrew” motion depends on the magnetic moment and therefore, on the amount of particles painted onto the swimmers surface. Also the uniformity of the coating influences the steerability.

In order to find a rotatable swimmer the magnetization of the object is a critical parameter, which can be increased by the choice of particles and the amount of lacquer. Since full rotation of the swimmer was achieved, the magnetization of the swimmer was sufficient when applying the maximal focus field strength (18 mT). When using other particles or another particle to paint ratio, the magnetic properties of the swimmer change and thus, the swimmer dynamics change. Moreover, the friction of the swimmer depends on its size and shape. These parameters also have an impact on the swimmer dynamics.

4.2. Visualization

The signal to background ratio (SBR) of the coated swimmer in comparision to the pure particle sample is shown in Fig. 5. It can be expected that the swimmer can be imaged since harmonics up to approximately 350 kHz are above an SBR of five, which indicates significance of the measured signal according to [35]. The MPI signal of the coated swimmer depends on the amount of Perimag painted onto the swimmer surface. The swimmer signal cannot be quantified in terms of iron particles since neither the total amount of Perimag particles in the coating nor the homogeneity of the paint layer is precisely known. Furthermore, a drop in signal intensity is expected for particles trapped in the coating [36]. The reconstructed images of the moving swimmer are shown in Fig. 6. While the exact shape of the swimmer is not reproduced in the images as a consequence of the low signal intensity, its forward movement is clearly visible in the data at a quality that is sufficient for tracking. Since the FFP position resides close to the swimmer location during the imaging sequence and the imaging frequencies are too high to overcome the scanners inertia, no swimmer movement is expected during imaging phase, as testified by video still imaging taken before and after the imaging sequence.

The exact shape of the swimmer is not represented by the images, however the forward movement can be clearly visualized. This information would suffice for tracking the swimmer. The location of the swimmer was observed before and after an imaging sequence with a video camera. It can be expected that the swimmer did not move during the imaging sequence. The force on an object due to the gradient field

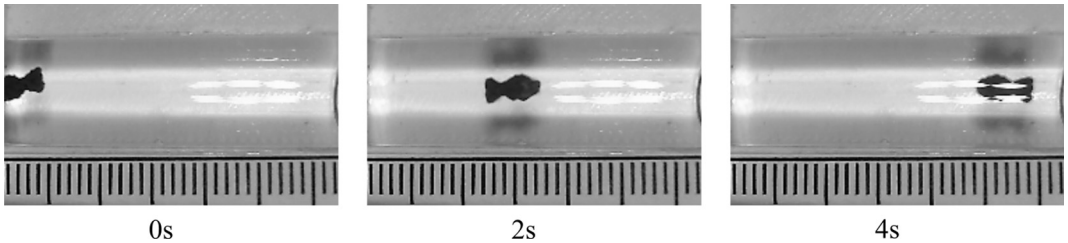

Fig. 3. Axial movement of the swimmer within 4 s at a frequency of 10 Hz and 18 mT focus field strength. It travels with a speed of approximately 6 mm/s. A video can be found in the Supplementary material [video:SwimmerGlasPhantom].

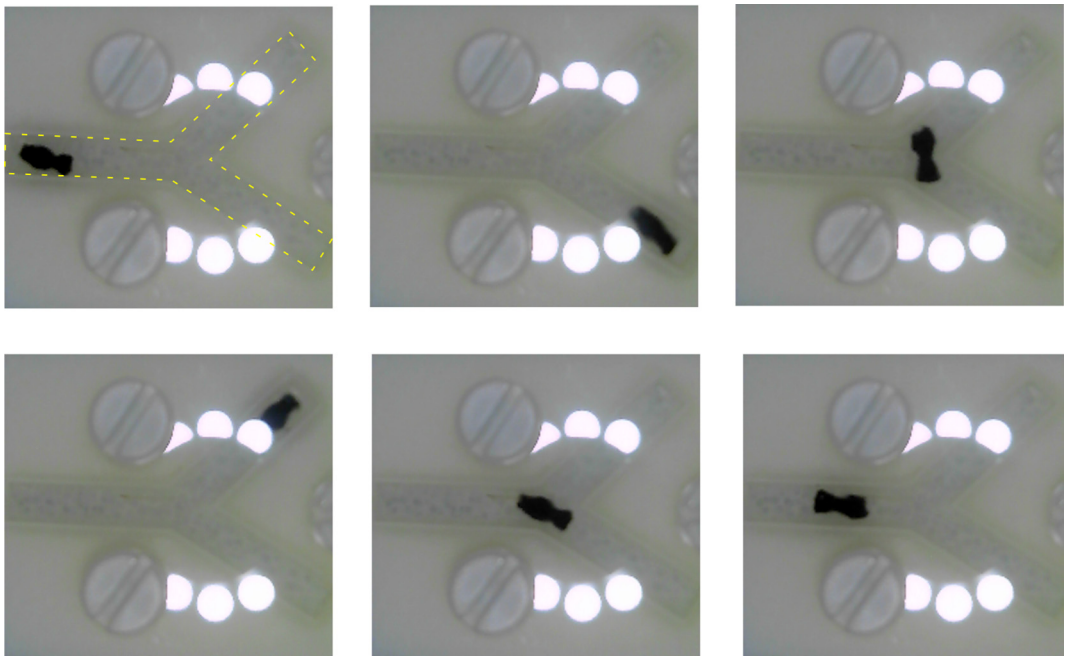

Fig. 4. Movement of the swimmer inside a vessel phantom steered with a frequency of 10 Hz and 18 mT focus field strength. The video can be found in the Supplementary material [video:SwimmerVesselPhantom].

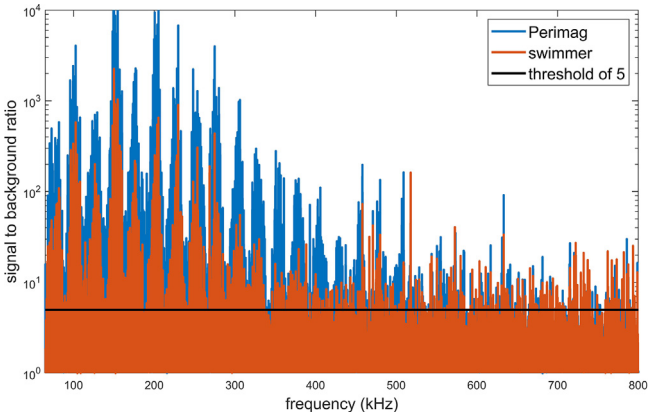

Fig. 5. The signal to background ratio of the swimmer in comparison to 10 µl undiluted Perimag. The data was acquired with a drive field in the x-, y- and z-direction. A threshold of five is indicated. Note, that a quantitative comparison between Perimag and the swimmer is not possible, since the iron concentration of the coating and the amount of paint is not known.

depends on the distance to the FFP. The swimmer is very close to the FFP during image acquisition, hence the force is expected to be very small. Since the FFP movement is very fast it is expected that the swimmer's inertia is sufficiently large such that it does not follow the varying magnetic field during an imaging sequence.

5. Conclusion

It has been demonstrated, that a swimmer coated with magnetic nanoparticles, can be actuated inside an MPI scanner. The focus fields of the MPI scanner were used to rotate a homogeneous magnetic field, which led to a rotation of the swimmer within a frequency range of up to 14 Hz. Similar to other micro swimmers [28,29], this swimmer showed the same swimming dynamics: a "corkscrew" motion was observed in the frequency range between 8 Hz and 14 Hz. The swimmer fulfilled a "wobbling" motion for smaller frequencies and no rotation was observed for frequencies larger than 14 Hz. A velocity of approximately 6 mm/s was observed at a rotation frequency of 10 Hz. The steerability of the swimmer through a Y-shaped vessel phantom showed the ability of the swimmer to be used e.g. as a transporter for therapeutics through the vascular system. This would enable to deliver drugs locally to regions difficult to access. Furthermore, the SBR showed the suitability of the swimmer to be imaged with MPI (see Fig. 5). First MPI images of the moving swimmer could be shown (see Fig. 6).

6. Outlook

In the future, the aim is to actuate and image the movement of the swimmer simultaneously. For this, the delay time between imaging and actuation mode needs to be reduced dramatically. For medical applications, e.g. to steer the swimmer inside the vascular system, the size of the swimmer needs to be reduced. This requires at first smaller bare swimmers, for which the size is limited by the resolution of the 3D-printer. It is planned to miniaturize the swimmer by using another 3D-printer. As the coating of smaller swimmers is a difficult task, different coating techniques need to be investigated. Since the steerability of the swimmer depends on its magnetic properties, further investigations on different kinds of particles and particle concentrations would be beneficial. A systematic analysis on the correlation between properties of different kinds of particles and the suitability for manipulation would improve the understanding of the observed swimmer dynamics. Also, a simulation study on the expected velocities in dependency of the rotation frequency is planned. It aims at establishing a more general relationship between the generated magnetic force and the swimmer's shape and size, taking into account the magnetic field strength, the magnet moment of the swimmer and the viscous friction which increases with rotation frequency. These parameters define the frequency regimes in which full rotation of the swimmer can be expected.

Acknowledgment

The authors gratefully acknowledge the Federal Ministry of Education and Research, Germany (BMBF) for funding this project under Grant Nos. 13GW0069A, 13GW0071D and 01DL17010A, as well

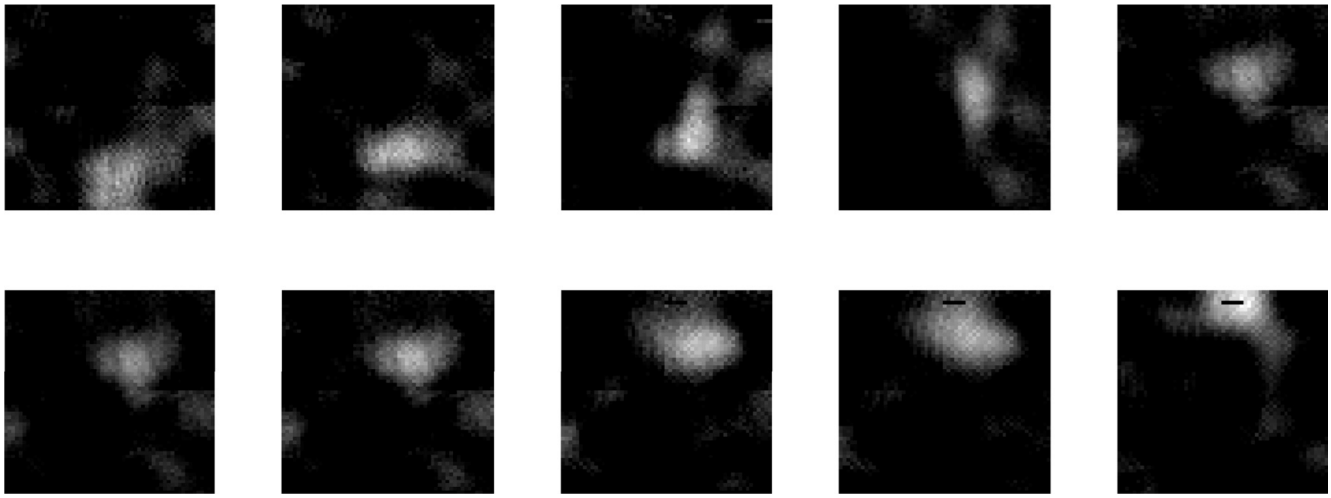

Fig. 6. MPI of a swimmer. From left to right, up to down: An image was acquired every 10 turns of the swimmer. In the actuation mode, the rotation frequency of the homogeneous magnetic field was 10 Hz and 18 mT focus field strength. In the imaging mode, the drive field strength was 12 mT, the gradient field 0.75 T/m in the x- and y-direction, and the FOV 32×32 mm^2. The images are reconstructed by use of a 57×57 system matrix. Right bottom: schematic draw of the swimmer with the size of 1.8 mm diameter and 4.5 mm length in the FOV.

as the German Research Foundation (DFG) under Grant No. BU 1436/7-1.

Appendix A. Supplementary data

Supplementary data associated with this article can be found, in the online version, athttps://doi.org/10.1016/j.jmmm.2018.10.056.

References

[1] S. Yim, M. Sitti, Design and rolling locomotion of a magnetically actuated soft capsule endoscope, IEEE Trans. Rob. 28 (1) (2012) 183–194, https://doi.org/10.1109/tro.2011.2163861.

[2] F. Munoz, G. Alici, W. Li, A review of drug delivery systems for capsule endoscopy, Adv. Drug Delivery Rev. 71 (2014) 77–85, https://doi.org/10.1016/j.addr.2013.12.007.

[3] F. Carpi, N. Kastelein, M. Talcott, C. Pappone, Magnetically controllable gastrointestinal steering of video capsules, IEEE Trans. Bio-medical Eng. 58 (2011) 231–234, https://doi.org/10.1109/TBME.2010.2087332.

[4] T.D. Than, G. Alici, H. Zhou, W. Li, A review of localization systems for robotic endoscopic capsules, IEEE Trans. Bio-medical Eng. 59 (2012) 2387–2399, https://doi.org/10.1109/TBME.2012.2201715.

[5] S. Yim, E. Gultepe, D.H. Gracias, M. Sitti, Biopsy using a magnetic capsule endoscope carrying, releasing, and retrieving untethered microgrippers, IEEE Trans. Biomedical Eng. 61 (2014) 513–521, https://doi.org/10.1109/TBME.2013.2283369.

[6] M. Simi, G. Gerboni, A. Menciassi, P. Valdastri, Magnetic torsion spring mechanism for a wireless biopsy capsule, J. Med. Devices 7 (4) (2013) 041009, https://doi.org/10.1115/1.4025185.

[7] S. Park, K. in Koo, S.M. Bang, J.Y. Park, S.Y. Song, D.D. Cho, A novel microactuator for microbiopsy in capsular endoscopes, J. Micromech. Microeng. 18 (2) (2008) 025032, https://doi.org/10.1088/0960-1317/18/2/025032.

[8] B.J. Nelson, I.K. Kaliakatsos, J.J. Abbott, Microrobots for minimally invasive medicine, Annu. Rev. Biomed. Eng. 12 (1) (2010) 55–85, https://doi.org/10.1146/annurev-bioeng-010510-103409.

[9] S. Tottori, L. Zhang, F. Qiu, K.K. Krawczyk, A. Franco-Obregón, B.J. Nelson, Magnetic helical micromachines: fabrication, controlled swimming, and cargo transport, Adv. Mater. 24 (6) (2012) 811–816, https://doi.org/10.1002/adma.201103818.

[10] M. Suter, L. Zhang, E.C. Siringil, C. Peters, T. Luehmann, O. Ergeneman, K.E. Peyer, B.J. Nelson, C. Hierold, Superparamagnetic microrobots: fabrication by two-photon polymerization and biocompatibility, Biomed. Microdevices 15 (6) (2013) 997–1003, https://doi.org/10.1007/s10544-013-9791-7.

[11] X. Yan, Q. Zhou, J. Yu, T. Xu, Y. Deng, T. Tang, Q. Feng, L. Bian, Y. Zhang, A. Ferreira, L. Zhang, Magnetite nanostructured porous hollow helical microswimmers for targeted delivery, Adv. Funct. Mater. 25 (33) (2015) 5333–5342, https://doi.org/10.1002/adfm.201502248.

[12] A. Ghosh, P. Fischer, Controlled propulsion of artificial magnetic nanostructured propellers, Nano Lett. 9 (6) (2009) 2243–2245, https://doi.org/10.1021/nl900186w.

[13] M. Medina-Sánchez, L. Schwarz, A.K. Meyer, F. Hebenstreit, O.G. Schmidt, Cellular cargo delivery: toward assisted fertilization by sperm-carrying micromotors, Nano Lett. 16 (1) (2015) 555–561, https://doi.org/10.1021/acs.nanolett.5b04221.

[14] B. Gleich, J. Weizenecker, Tomographic imaging using the nonlinear response of magnetic particles, Nature 435 (7046) (2005) 1214–1217, https://doi.org/10.1038/nature03808.

[15] J. Weizenecker, B. Gleich, J. Rahmer, H. Dahnke, J. Borgert, Three-dimensional real-time in vivo magnetic particle imaging, Phys. Med. Biol. 54 (5) (2009) L1–L10, https://doi.org/10.1088/0031-9155/54/5/l01.

[16] A. Mahmood, M. Dadkhah Tehrani, M. Ok Kim, J. Yoon, A novel design of an MPI-based guidance system for simultaneous actuation and monitoring of magnetic nanoparticles, IEEE Trans. Magn. 51 (2015) 1–5, https://doi.org/10.1109/TMAG.2014.2358252.

[17] T. Kuboyabu, A. Ohki, N. Banura, K. Murase, Usefulness of magnetic particle imaging for monitoring the effect of magnetic targeting, Open J. Med. Imaging 06 (02) (2016) 33–41, https://doi.org/10.4236/ojmi.2016.62004.

[18] T.-A. Le, X. Zhang, A.K. Hoshiar, J. Yoon, Real-time two-dimensional magnetic particle imaging for electromagnetic navigation in targeted drug delivery, Sensors 17 (9) (2017) 2050, https://doi.org/10.3390/s17092050.

[19] X. Zhang, T.-A. Le, J. Yoon, Development of a real time imaging-based guidance system of magnetic nanoparticles for targeted drug delivery, J. Magn. Magn. Mater. 427 (2017) 345–351, https://doi.org/10.1016/j.jmmm.2016.10.056.

[20] F. Griese, P. Ludewig, F. Thieben, N. Gdaniec, T. Knopp, Imaging and moving magnetic beads with magnetic particle imaging for targeted drug delivery, in: 2018 IEEE 15th International Symposium on Biomedical Imaging (ISBI 2018), IEEE, 2018.https://doi.org/10.1109/isbi.2018.8363808.

[21] N. Nothnagel, J. Rahmer, B. Gleich, A. Halkola, T.M. Buzug, J. Borgert, Steering of magnetic devices with a magnetic particle imaging system, IEEE Trans. Biomed. Eng. 63 (11) (2016) 2286–2293, https://doi.org/10.1109/TBME.2016.2524070.

[22] J. Rahmer, D. Wirtz, C. Bontus, J. Borgert, B. Gleich, Interactive magnetic catheter steering with 3-d real-time feedback using multi-color magnetic particle imaging, IEEE Trans. Med. Imaging 36 (2017) 1449–1456, https://doi.org/10.1109/TMI.2017.2679099.

[23] J. Rahmer, C. Stehning, B. Gleich, Spatially selective remote magnetic actuation of identical helical micromachines, Sci. Rob. 2 (3) (2017) 2845, https://doi.org/10.1126/scirobotics.aal2845.

[24] J. Rahmer, C. Stehning, B. Gleich, Remote magnetic actuation using a clinical scale system, PLOS ONE 13 (3) (2018) e0193546, https://doi.org/10.1371/journal.pone.0193546.

[25] J.J. Abbott, O. Ergeneman, M.P. Kummer, A.M. Hirt, B.J. Nelson, Modeling magnetic torque and force for controlled manipulation of soft-magnetic bodies, IEEE Trans. Rob. 23 (6) (2007) 1247–1252, https://doi.org/10.1109/tro.2007.910775.

[26] M. Sitti, H. Ceylan, W. Hu, J. Giltinan, M. Turan, S. Yim, E. Diller, Biomedical applications of untethered mobile milli/microrobots, Proc. IEEE 103 (2) (2015) 205–224, https://doi.org/10.1109/jproc.2014.2385105.

[27] K. Bente, A. Codutti, F. Bachmann, D. Faivre, Biohybrid and bioinspired magnetic microswimmers, Small (2018) 1704374, https://doi.org/10.1002/smll.201704374.

[28] A. Ghosh, P. Mandal, S. Karmakar, A. Ghosh, Analytical theory and stability analysis of an elongated nanoscale object under external torque, PCCP 15 (26) (2013) 10817, https://doi.org/10.1039/c3cp50701g.

[29] K.I. Morozov, A.M. Leshansky, Dynamics and polarization of superparamagnetic chiral nanomotors in a rotating magnetic field, Nanoscale 6 (20) (2014) 12142–12150, https://doi.org/10.1039/c4nr02953d.

[30] J. Haegele, T. Sattel, M. Erbe, K. Luedtke-Buzug, M. Taupitz, J. Borgert, T. Buzug, J. Barkhausen, F. Vogt, Magnetic particle imaging (MPI), RöFo – Fortschritte auf dem Gebiet der Röntgenstrahlen und der bildgebenden Verfahren 184 (05) (2011) 420–426, https://doi.org/10.1055/s-0031-1281981.

[31] T. Knopp, T.M. Buzug, Magnetic Particle Imaging: An Introduction to Imaging

Principles and Scanner Instrumentation, Springer, Berlin/Heidelberg, 2012, https://doi.org/10.1007/978-3-642-04199-0.
[32] M. Graeser, T. Knopp, P. Szwargulski, T. Friedrich, A. von Gladiss, M. Kaul, K.M. Krishnan, H. Ittrich, G. Adam, T.M. Buzug, Towards picogram detection of superparamagnetic iron-oxide particles using a gradiometric receive coil, Sci. Rep. 7 (1) (2017), https://doi.org/10.1038/s41598-017-06992-5.
[33] M. Grüttner, T. Knopp, J. Franke, M. Heidenreich, J. Rahmer, A. Halkola, C. Kaethner, J. Borgert, T. Buzug, On the formulation of the image reconstruction problem in magnetic particle imaging, Biomedizinische Technik/Biomed. Eng. 58 (6) (2013) 583–591, https://doi.org/10.1515/bmt-2012-0063.
[34] I. Schmale, J. Rahmer, B. Gleich, J. Kanzenbach, J.D. Schmidt, C. Bontus, O. Woywode, J. Borgert, First phantom and in vivo MPI images with an extended field of view, in: J.B. Weaver, R.C. Molthen (Eds.), Medical Imaging 2011: Biomedical Applications in Molecular, Structural, and Functional Imaging, SPIE, 2011.https://doi.org/10.1117/12.877339.
[35] A. Rose, The sensitivity performance of the human eye on an absolute scale, J. Opt. Soc. Am. 38 (1948) 196–208.
[36] H. Remmer, E. Roeben, A.M. Schmidt, M. Schilling, F. Ludwig, Dynamics of magnetic nanoparticles in viscoelastic media, J. Magn. Magn. Mater. 427 (2017) 331–335, https://doi.org/10.1016/j.jmmm.2016.10.075.